Energy Conversion and Management 357 (2026) 121439

Contents lists available at ScienceDirect

Energy Conversion and Management

journal homepage: www.elsevier.com/locate/enconman

Research Paper

Low-carbon power generation using DME: A thermodynamic assessment of two DME-fueled sCO_2 oxy-combustion power cycles

Ghadi Abi Haidar [a], Philipp Morsch [a,*], Andreas Peschel [a,b]

[a] Forschungszentrum Jülich GmbH, Institute for a Sustainable Hydrogen Economy (IHE), Jülich, Germany
[b] RWTH Aachen University, Aachener Verfahrenstechnik, Process and Plant Engineering for Chemical Hydrogen Storage, Aachen, Germany

ARTICLE INFO

Keywords:
DME
Hydrogen carrier
Oxy combustion
sCO_2
Allam cycle
Carbon neutral power generation
Carbon capture

ABSTRACT

Supercritical carbon dioxide (sCO_2)-based oxy-combustion power cycles, such as the Allam cycle, enable high-efficiency power generation with integrated carbon capture without the need for additional amine-based scrubbing plant. While these cycles are mostly discussed in combination with fossil fuels, the use of a renewable chemical hydrogen carrier, dimethyl ether (DME), remains largely unexplored. Besides its good combustion characteristics, DME offers the potential to establish a circular carbon loop when recycling the captured CO_2 for DME-synthesis. This study evaluates DME as a fuel in the Allam cycle and benchmarks its thermodynamic performance against a natural gas-fired configuration under consistent system boundaries. The results show that the DME-fueled Allam cycle achieves a net efficiency of 50.4 % and an effective CO_2 capture rate exceeding 96 %, comparable to the natural gas-fired reference. These findings highlight DME as a promising fuel for sCO_2 oxy-combustion cycles Building on the integration of DME, a modified configuration, the Liquefied Recycle Allam Cycle (LiRAC), is proposed. The LiRAC integrates a vapor compression unit using DME as refrigerant to fully liquefy the CO_2-rich working medium. This enables pump-based pressurization, reduces the energy demand associated with downstream CO_2 conditioning, and delivers most of the purified CO_2 in liquid form. The LiRAC achieves a net efficiency of 48.7 % while maintaining high CO_2 capture rates, demonstrating the feasibility of liquefied working-medium schemes and motivating further optimization and part-load assessment.

1. Introduction

Global demand for electricity continues to rise, driven by increasing electrification and consumption [1,2]. Although renewable energy capacity is growing, the uneven distribution of these resources across regions and over time requires energy systems that can transfer energy over long distances, store it for extended periods, and ensure stable electrical-grid operation.

Chemical hydrogen carriers, such as dimethyl ether (DME) produced from renewable electricity, are a promising option for bridging regional and temporal renewable electricity supply and demand imbalances [3]. DME, synthesized from CO_2 and green hydrogen, has a high energy density and a relatively high hydrogen content compared to alternative hydrogen carriers such as methanol, ammonia and liquid organic hydrogen carriers [4,5]. Furthermore, the transport and handling of DME are comparable to liquefied petroleum gas [6], potentially allowing the use of existing infrastructure. At the destination, hydrogen may either be extracted from DME via steam reforming, or DME may be used directly in industrial processes [5,7].

For instance, its favorable combustion characteristics make DME a suitable renewable fuel for thermal power stations [8,9], generating on-demand heat and electricity in regions with energy deficits and thus stabilizing electricity grids. However, using DME as an energy vector to address regional variability and electrical-grid instabilities requires a circular carbon path to be established by recycling generated CO_2 from power generation for the DME-synthesis, thus enabling sustainable CO_2 deployment and securing feedstock [6]. Fortunately, logistical advantages for the carbon loop arise from the ability to transport CO_2 and DME in the same vessel systems [10–12]. Still, the power cycle must enable high carbon capture rates while maintaining high efficiencies.

The state-of-the-art are natural gas (NG)-fueled combined gas turbine cycles equipped with solvent-based post-combustion carbon capture (NGCC-PCC) can achieve high capture rates, but the cycle's net efficiency is heavily influenced by the capture rate and the conditioning of captured CO_2 [13–16]. In contrast, emerging oxy-combustion supercritical CO_2 (sCO_2) cycles, such as the Allam cycle [17], offer an alternative approach by integrating CO_2 capture into the process, thus

* Corresponding author at: Forschungszentrum Jülich GmbH, Institute for a Sustainable Hydrogen Economy (IHE), Jülich, Germany.
E-mail address: p.morsch@fz-juelich.de (P. Morsch).

https://doi.org/10.1016/j.enconman.2026.121439
Received 30 January 2026; Received in revised form 30 March 2026; Accepted 31 March 2026
Available online 6 April 2026

Nomenclature

Abbreviations

CC	Carbon capture
CMP	Compressor
COL	Distillation column
CPU	Compression and purification unit
DME	Dimethyl ether
EL	Electrical
FL	Flash drum
HX	Heat exchanger
KPI	Key performance indicator
LHV	Lower heating value
LiRAC	Liquefied recycle Allam cycle
LNG	Liquefied natural gas
LPG	Liquefied petroleum gas
NGCC	Natural gas combined cycle
OX	Oxidant mixture
PCC	Post-combustion carbon capture
PMP	Pump
REC	Recuperator
RCL	Recycle
REB	Reboiler
sCO_2	Supercritical carbon dioxide
SI	Supplementary information
VCU	Vapor compression unit
VLV	Valve
WT	Water

Subscripts

c	Compressor
cond	Condenser
el	Electrical
in	Inlet
m	Mechanical
out	Outlet
p	Pump
RCL	Recycle
sat	Saturation
T	Turbine
th	Thermal

Symbols

DH	Enthalpy difference (relative to reference state)
H	Enthalpy
LF	Liquid fraction
$\dot{m}$	Mass flow rate
p	Pressure
P	Power
$\dot{Q}$	Heat flow
S	Entropy
T	Temperature
VF	Vapor fraction
V	Volumetric flow rate
w	Specific work
ρ	Density
η	Efficiency

avoiding the need for large, solvent-based PCC plants and facilitating CO_2 conditioning. These sCO_2 cycles also allow for the use of compact equipment, potentially reducing capital costs and footprint [18]. The Allam cycle demonstrates high efficiency with favorable economics and has a high technology readiness level among sCO_2 oxy-combustion power cycles, supported by a demonstration plant and further projects under development [17,19–21].

A broad range of studies has evaluated the performance of oxy-combustion sCO_2 cycles. The IEAGHG comparison study established a consistent reference framework for several configurations [19], followed by Rogalev et al. [22] who provided a comprehensive overview of closed and semi-closed sCO_2 cycles. Among these cycles, the NG-fueled Allam cycle has repeatedly demonstrated competitive efficiency and low levelized cost of electricity [17,21]. A broader set of Allam cycle simulation studies, covering variations in configuration, boundary conditions, and design assumptions, is summarized separately in Table S10 in the Supplementary Information (SI).

Concerning carbon capture within the Allam cycle, some studies excluded purification of the captured CO_2 entirely, while others assumed low purity levels suitable only for enhanced oil recovery (EOR) applications, often with a compression and purification unit (CPU) recovery rate around 90 %. With the rapid increase in large-scale CO_2 transport projects [11,23], transport specifications are becoming more stringent, highlighting the importance of explicitly modeling CO_2 purification at high purity and recovery rates.

In this context, Martinelli et. al. [24] investigated the NG-fueled Allam cycle in its standard configuration with an integrated hybrid flash-distillation CO_2 purification unit, targeting high capture rates and pipeline-quality CO_2. Using preliminary design correlations, they reported net electric efficiencies between 48.7 % and 56.1 % depending on plant scale and the amount of recoverable and additional external heat.

Despite the research progress, comparing reported efficiencies remains challenging because of the different assumptions, configurations, and process boundaries. Most studies focus on NG or liquefied natural gas (LNG), with only limited work on alternative fuels. Manente et al. [25] presented a methanol-fueled Allam cycle integrated with an e-methanol synthesis plant and an electrolyzer producing both hydrogen and oxygen. Under their modeling assumptions, without considering further purification of the captured CO_2, the methanol-fired cycle achieves a net thermal efficiency of 52.95 %, which is less than one percentage point below the NG-fueled case. Furthermore, Dong et. al [26] proposed a DME-fueled dual expansion and triple recuperation cycle (DETRC) with CFD-based combustion modeling. Their study reported high thermal and exergy efficiencies and identified the optimal operating ranges for the DETRC. Compared with NG, their study indicated a lower specific oxygen demand for DME combustion. However, a direct comparison between DME- and NG-fueled Allam cycles under identical assumptions has not been addressed.

In summary, research has primarily focused on NG-fueled Allam cycles, whereas the potential of DME remains largely unexplored. In the context of DME being a potential future hydrogen transport vector, this paper investigates the potential of DME as fuel in sCO_2 oxy-combustion cycles. Specifically, we benchmark DME- and NG-fueled Allam cycles under aligned assumptions and coupled with detailed distillation-based CPU models to quantify their energetic impact while achieving CO_2 product purity aligned with ISO 27913 requirements for dense-phase pipeline transportation [27]. Additionally, we introduce a modified Allam cycle, the Liquefied Recycle Allam Cycle (LiRAC), which explores how DME's thermophysical properties can support a reconfiguration of the Allam cycle. The modification employs a vapor compression unit (VCU) with DME as fuel and as the refrigerant to fully liquefy the working medium. The thermodynamic performance of the DME-fueled Allam and LiRAC is evaluated through mass and energy balances and heat-recuperation analyses.

2. System description

The power cycles considered in this work are semi-closed sCO_2 oxy-combustion power cycles. Combustion occurs in a CO_2-diluted atmosphere using high-purity oxygen supplied by an air separation unit (ASU). This produces a working fluid that is mainly composed of CO_2 and water (H_2O). Water can be condensed and extracted leading to a remaining high-purity CO_2 working fluid. This high purity CO_2 can be extracted and captured, thus enabling an integrated carbon capture into the cycle without the need for the solvent-based post-combustion separation which is required in conventional air-fired systems with nitrogen dilution [18]. The ASU's electricity demand contributes to the system's overall efficiency. Consequently, the amount of oxygen required for the combustion of the fuel directly influences system performance. In this context, dimethyl ether (DME) has a comparatively lower stoichiometric oxygen demand per unit of lower heating value than alternatives hydrogen carriers such as Methanol (see Table S18 in SI).

The simplified process flow diagrams of the DME-fueled Allam and LiRAC are illustrated together in Fig. 1, to facilitate the differentiation between the cycles. In addition, a pressure-enthalpy diagram of both cycles is illustrated in Fig. 2, to further enhance the reader's comprehension of the thermodynamic differences between them. Moreover, the conditioning and purification of the captured CO_2 is investigated in this work through the simulation of two different CPU configurations. CPU-1 is integrated into the Allam cycle (cf. Fig. 4), and CPU-2 into the LiRAC (cf. Fig. 5). Both CPUs are described in section 3.

2.1. DME-fueled Allam cycle

Various configurations of the Allam cycle have been explored in previous studies and patents, each varying in technical scope and design assumptions. In this work, the Allam cycle is modeled based on the assumptions of the IEAGHG [19] and Scaccabarozzi et al. [28]. The corresponding process flow is depicted by the blue lines in Fig. 1 and Fig. 2, while detailed stream data are provided in Table A5 in the Appendix.

The fuel DME (stream 1) is first compressed to high pressure before entering the combustion chamber where the combustion occurs with 3 % excess of oxygen relative to the stoichiometric ratio. CO_2 is used as a diluent to control the combustion temperature at 1150 °C. Consequently, the combustion product (stream 4) consists mainly of CO_2 and water.

After combustion, the working fluid enters the turbines at 300 bar and 1150 °C. Part of the CO_2 diluent is used (stream 11) as cooling flow to limit the blade temperature to 860 °C. In the turbine, the working fluid expands to 34 bar (stream 5). It further enters the recuperator at 742 °C, where it cools to 57 °C by heating the incoming oxidant and CO_2 diluent streams entering the combustor (stream 9 and 10). Additionally, hot air at 273 °C from the ASU compressors provides supplementary heat to the system via the recuperator.

Following the recuperation, stream 6 is further cooled to 26 °C enabling water condensation and separation. Part of the stream is then sent to CPU-1, while the remaining is recycled and used as CO_2 diluent. Thereafter, the recycled CO_2 is first compressed in a four-stage intercooled compressor to 100 bar, beyond the critical point, then cooled to 26 °C achieving a dense phase and further pumped to 120 bar. Subsequently, part of the recycled CO_2 is mixed with the oxygen feed to form an oxidant flow with 13.34 mol% O_2 [19]. Finally, the oxidant stream and the recycled diluent are further pumped to 305 bar and preheated in the recuperator (streams 2 and 3), before entering the combustion chamber. At these operating conditions, the CO_2-rich working fluid

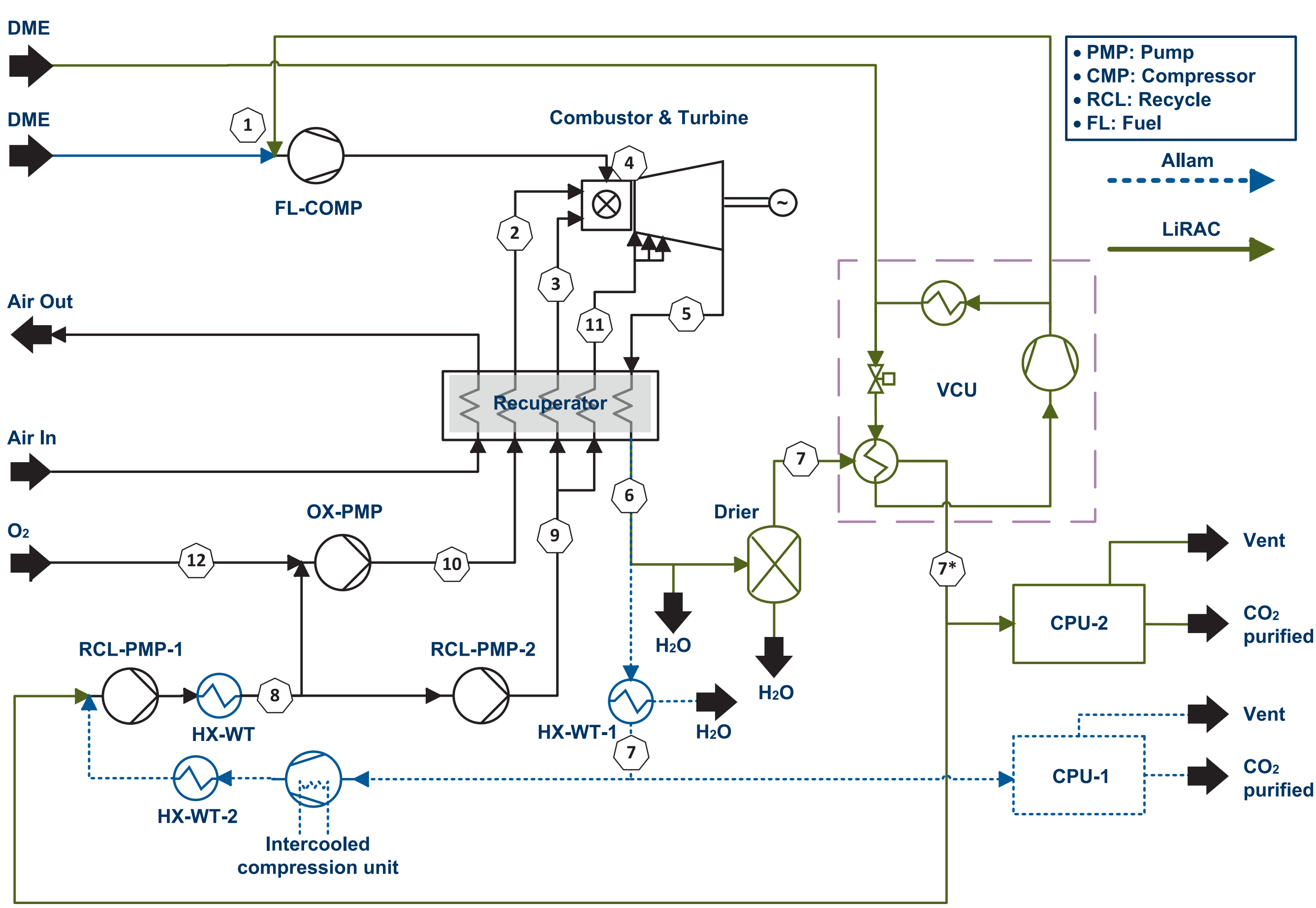

Fig. 1. Simplified process flow diagram (PFD) of the simulated power generation cycles. The blue dotted line represents the Allam cycle, while the green line represents the LiRAC. A detailed stream summary of the numerated streams is provided in Table A5.

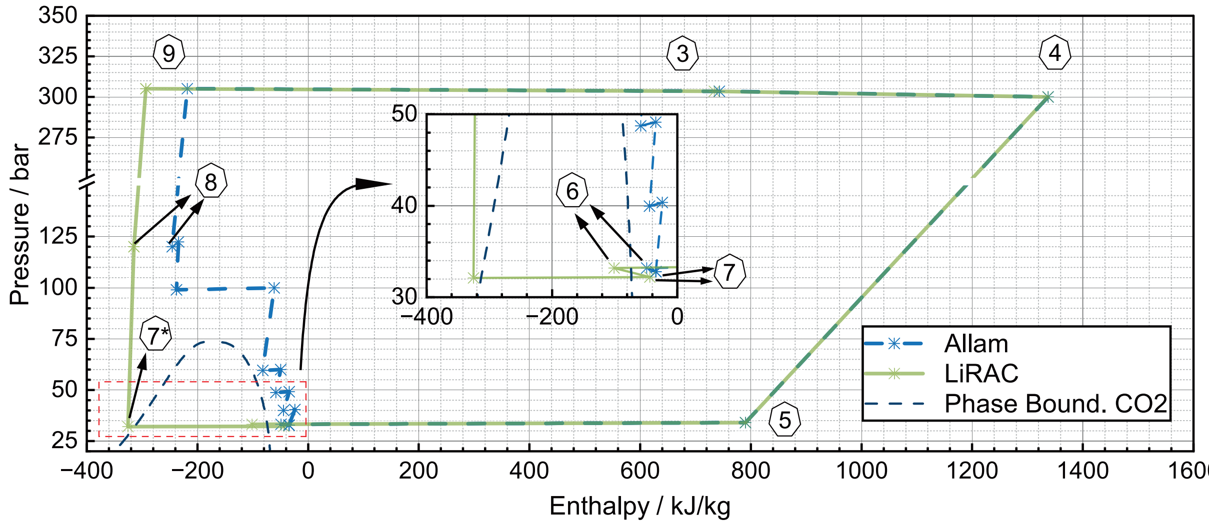

Fig. 2. Pressure-enthalpy diagram of the simulated cycles. The enthalpy reference is set to 25 °C and 1 bar (enthalpy of formation).

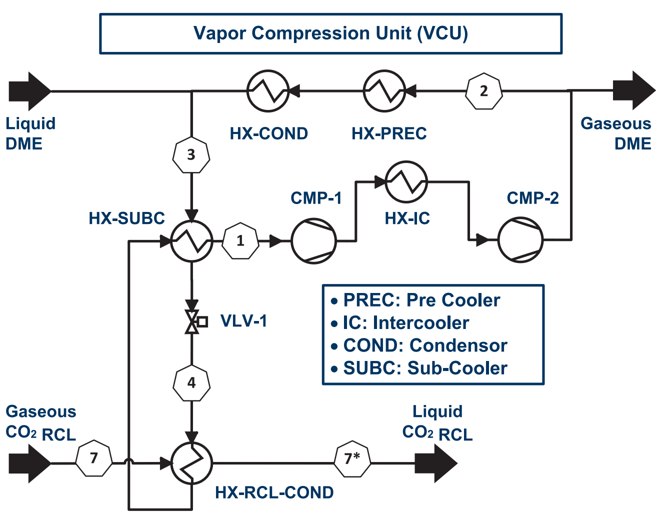

Fig. 3. Simplified process flow diagram of the vapor compression unit (VCU) integrated into the LiRAC.

exhibits high density and remains far from the two-phase region, enabling efficient pressurization while avoiding condensation. In addition, it provides favorable heat transfer properties, allowing a high degree of internal heat recuperation enhancing cycle efficiency [29].

Since the cycle operates with a high recycle fraction of the working fluid, impurities introduced with the fuel and oxygen may accumulate in the process, affecting both overall system performance and the purity of the CO_2 stream supplied to the CPU. This, in turn, influences the power demand for downstream conditioning and purification. Consequently, fuel and oxidant purity, together with the combustion stoichiometry, are critical for limiting inert accumulation (e.g., N_2, Ar) and maintaining stable operation.

2.2. Liquified Recycle Allam Cycle – LiRAC

The LiRAC represents a modification of the Allam cycle where the recycled stream is fully liquefied. In this study, the LiRAC and Allam cycles are modeled under the same assumptions and process parameters. A simplified process flow diagram as well as the corresponding thermodynamic states are shown in green in Fig. 1 and Fig. 2. The main difference to the Allam cycle is the integration of a VCU for recycle stream liquefaction (Fig. 3, Fig. 9), using the DME as both, fuel and refrigerant.

A key step in the Allam cycle is pressurization of the CO_2-rich recycled stream. The recycled stream is first compressed above the critical point and cooled to ambient temperature using cooling water. As a result, the stream reaches a dense, supercritical state, allowing for efficient further pressurization by a pump rather than a compressor. This combination of compressors and pumps significantly reduces the energy required for pressurization. However, these steps heavily depend on the mixture's critical point and ambient cooling conditions. Furthermore, the cycle operates in a semi-closed configuration, the recycled working fluid directly connects the turbine outlet to the turbine inlet through the circulating mass flow. This coupling may create strong interdependencies between key process units within the recycle loop, including the turbine, recuperator, and compression system. As a result, variations in turbine operating conditions can propagate through the recycle loop and influence upstream process states. Such interactions may constrain ramping behavior during load changes and complicate control strategies. Similar control challenges have been reported for highly integrated sCO_2 power cycles in the literature [18,30–34].

Unlike the Allam cycle, the LiRAC uses subcritical liquefaction of the recycled stream at the cycle's lowest pressure. This enables the entire pressurization process to be achieved solely through pumping. In addition, passing through the two-phase region enables phase separation, allowing accumulated inerts to be vented from the working fluid and limiting their accumulation due to solubility limitations. Furthermore, the subcritical liquefaction ensures a dense phase at the pump inlet, regardless of the critical point. Consequently, the configuration may provide increased robustness against variations in the recycle stream composition arising from impurity accumulation during combustion and from inerts introduced with the oxygen feed. This, in turn, may reduce the oxygen feed purity requirements. Moreover, the LiRAC configuration enables integration of a raw liquid CO_2 buffer tank at stream 7*. This tank can partially decouple the CPU, VCU, and power cycle by interrupting the direct mass flow coupling. Therefore, the proposed configuration may facilitate smoother operation, improve part-load flexibility, and enable controlled CO_2 handling. Similar compressorless cycle concepts have been reported to potentially enable independent regulation of key operating parameters and operation over a wider range of operating conditions [35,36]. However, quantifying these potential operational advantages and potential implications of the VCU integration requires further part-load and dynamic investigations.

From a process perspective, the differences between the LiRAC and the Allam cycle begin with the partly condensed hot outlet from the recuperator outlet (stream 6). After the recuperator, the working fluid is

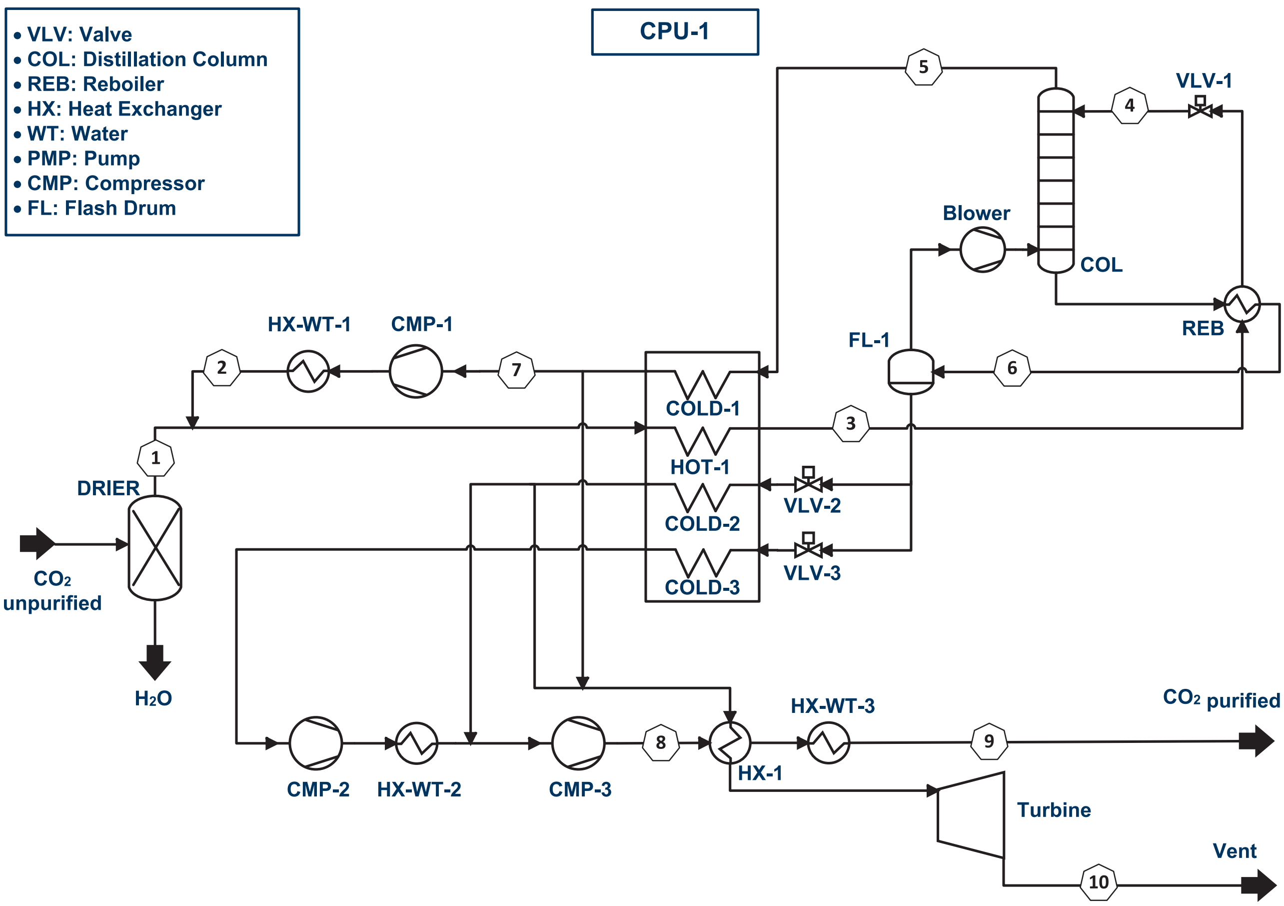

Fig. 4. Simplified process flow diagram of the compression and purification unit (CPU-1) used for the Allam cycle. The CO_2 purified aligns with ISO 27913 for dense phase pipeline transportation [27]. Stream Summary of the numerated streams is provided in Table S7 in SI.

dried to eliminate water and prevent ice formation. The dried gas (stream 7) enters the condenser of the VCU and is fully liquefied at −10 °C and 32.2 bar (stream 7*). Some of the liquid CO_2 is sent to the CPU, while the rest is recycled and pressurized by pumps thus simplifying the pressurization and potentially offering a potential for better operation [18,35,36]. The pressurized recycled working fluid enters the recuperator at a temperature of 11 °C compared to 50 °C in the case of the Allam cycle, leading to lower hot outlet temperature (see section 5.2.1).

2.3. Vapor compression unit

The VCU operates with its own refrigeration loop and uses the fuel DME as refrigerant. The process scheme of the VCU is represented in Fig. 3.

First, liquid fuel at 26 °C is added to the VCU's refrigeration loop. Then, the refrigerant is subcooled and throttled (stream 4) to 1.79 bar and −12 °C to ensure the necessary temperature difference in the evaporator. The process conditions and constraints achieved are strongly depending on the composition of the fuel-grade DME used. The refrigerant exits the evaporator with a high vapor fraction and then enters recuperative superheating by subcooling the incoming refrigerant (stream 3). After superheating, the refrigerant is compressed in an intercooled, two-step process to a saturation pressure of 6.9 bar (stream 2).

Following the compression, a portion of the refrigerant is sent as fuel to the power cycle's fuel compressor, while the rest is recycled in the VCU loop, where it is condensed at 26 °C using cooling water. Adding the fuel to the refrigeration system before the fuel compressor increases the cooling duty of the evaporator. However, the use of DME as both fuel and refrigerant requires consideration of the fuel composition, as fuel-grade specifications are not primarily defined for refrigerant applications.

3. Compression and purification

Although oxy-combustion produces CO_2-rich flue gas, residual inerts from the oxygen stream (e.g., N_2, Ar) and trace fuel impurities accumulate in the CO_2 rich stream. Therefore, further purification remains necessary, particularly for oxygen removal. The purification of the captured CO_2 is a critical step in meeting transport specifications and achieving high effective capture rates. However, several studies have investigated CPU configurations independently of the power cycle, making it difficult to understand its energetic impact on the overall net efficiency.

Posch et al. [37] examined two CPU types: a distillation-based system with and without external cooling and a double-flash configuration. They concluded that lower CO_2 content substantially increases power demand and cooling duty. The distillation-based system achieved higher purity than the double-flash configuration, though at a greater energy cost. Additionally, they found that higher feed pressure reduces cooling duty and improves separation performance without directly influencing CO_2 product purity.

Sala et al. [38] investigated six CPU concepts from a techno-economic perspective and showed that flash separation alone cannot achieve high purity, particularly with regard to oxygen. The highest purity and recovery were achieved using hybrid flash-distillation configurations.

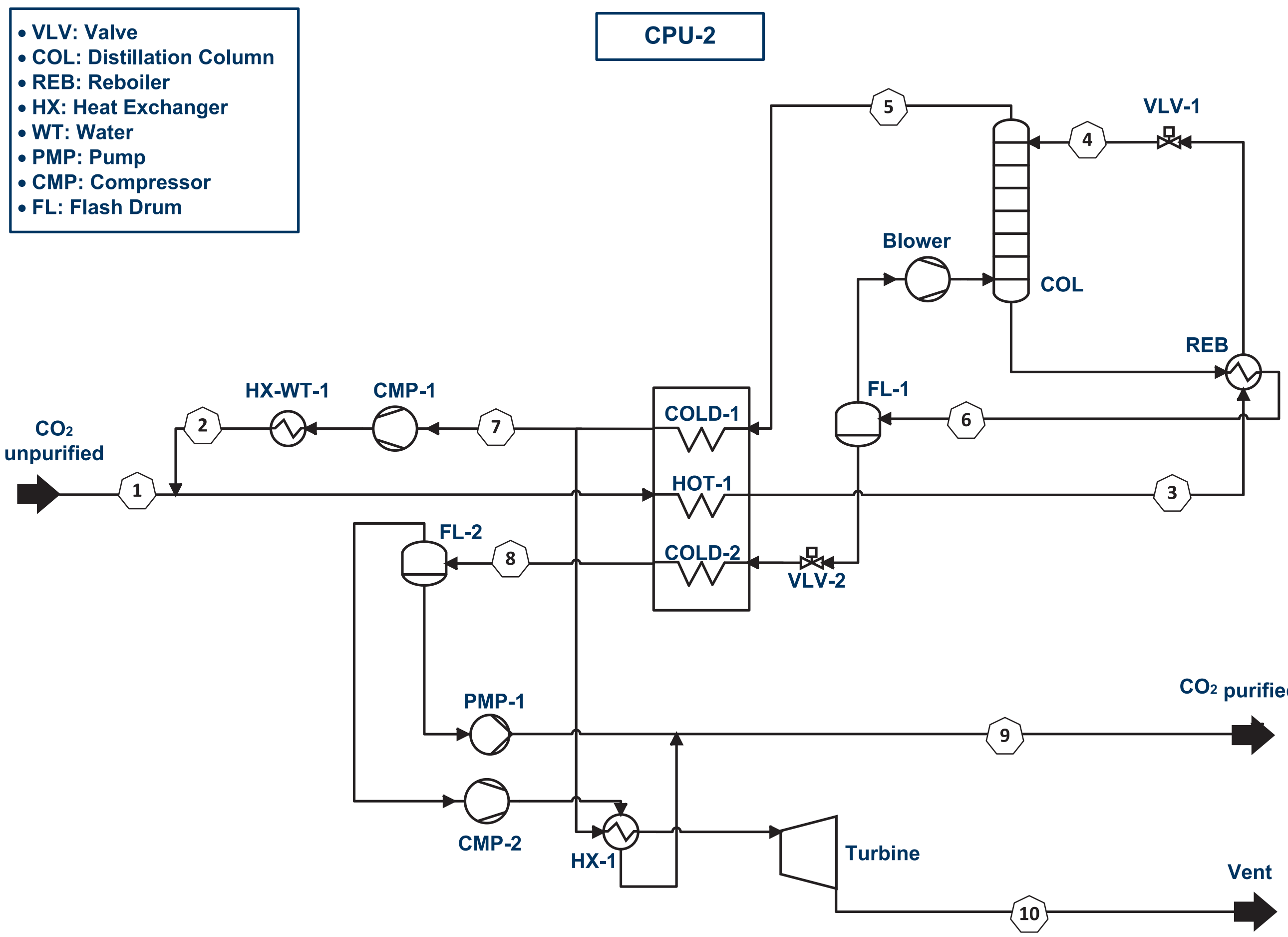

Fig. 5. Simplified process flow diagram of the compression and purification unit (CPU-2) used for the LiRAC.

The IEAGHG study [19] adopted the patented CPU design [39], demonstrating that a high-purity oxygen feed (99.5 mol %) in oxy-combustion cycles eliminates the need for a flash drum and enables achieving the target purity of EOR with a single distillation column.

The required CO_2 purity depends on the transport mode and project specifications. To support a standardized CO_2 infrastructure and enable circular carbon loop, captured CO_2 must meet the established purity and thermodynamic state guidelines. These guidelines include specifications for pipeline and geological storage [27,40], and for transportation by ship [12].

Key purity limitations relevant for oxy-combustion systems using gaseous fuels are summarized in Table 1. Oxygen is among the most restrictive impurities, with specifications requiring concentrations below 10 ppm mol. Meeting this limit places stringent demands on CPU design and operating conditions. This work ensures that the captured CO_2 aligns with the specification of the ISO 27913 for dense phase pipeline transportation [27].

3.1. Compression and purification unit 1

The CPU-1 used in this work for the Allam cycle is a distillation-based configuration with internal cooling configured in alignment with the literature [19,38]. Fig. 4 illustrates the process flow diagram, and Table S7 in SI provides the values of the streams.

After water condensation and separation in the power cycle, the CO_2 mixture is extracted and sent to the CPU as feed. A drying process first takes place to avoid ice formation. Then, the feed is mixed with a gaseous stream (stream 2) before entering the recuperator, where the

Table 1
Summary of essential CO_2 specifications from ISO standards and ongoing transport projects.

	ISO 27913–2016 [40]	ISO 27913–2024 [27,41]	ISO 27913–2024 [27,41]	IEAGHG–2015 [19]	Northern Lights–2024 [23]	Aramis–2025 [42]
Transport	Pipeline	Pipeline gas phase	Pipeline dense phase	Pipeline dense phase	Ship	Ship
Unit	mol	mol	mol	vol	mol	mol
CO_2	> 95 %	> 95 %	> 95 %	> 95 %	> 99.81 %	
O_2	*	< 10 ppm	< 10 ppm	< 100 ppm	< = 10 ppm	< 10 ppm
Ar	–	< 4 %	–	< 4 %	–	–
N_2	2 %	< 4 %	–	< 4 %	–	–
CO	0.2 %	< 0.2 %	< 0.7 %	< 0.2 %	<= 100 ppm	< 1200 ppm
H_2	0.75 %	< 1 %	< 1 %	< 4 %	<= 50 ppm	< 500 ppm
H_2O	20–630 ppm vol	< 50 ppm	< 630 ppm	< 50 ppm	<= 30 ppm	< 30 ppm
Methanol	–	< 350 ppm	–	–	–	< 40 ppm
Sum of inerts	< 4 %	< 4 %	< 5 %	< 4 %	–	< 2000 ppm

*: The amount of oxygen in the pipeline must be kept low enough to prevent acids, solids, and corrosion from damaging the pipeline over its lifetime.

stream is cooled and partially liquefied. After liquefaction, stream 3 enters the reboiler of the distillation column, providing heat.

Subsequent to the reboiler, the stream is throttled (stream 4) and enters the top of the distillation column, wherein phase separation occurs across a temperature range at constant pressure, producing high-purity liquid CO_2 at the bottom and gaseous waste at the top.

Both the gaseous stream from the top and the liquid stream from the bottom are used to provide the necessary cooling in the recuperator to liquefy the feed, thereby enabling internal recuperative refrigeration. The purified liquid CO_2 is throttled before entering the recuperator to ensure a temperature difference for heat transfer. After recuperation, a portion of the top waste stream (stream 7) is recycled, compressed, and cooled to 26 °C (stream 2). It is then mixed with the feed (stream 1), enhancing the CO_2 recovery and separation performance.

Ultimately, the pure CO_2 leaves the recuperator fully evaporated, is compressed to 110 bar, and is cooled to 26 °C (stream 9). Meanwhile, the hot waste stream expands in a turbine before being vented to the atmosphere (stream 10). Adding a portion of the pure, evaporated CO_2 to the waste stream could increase the turbine's power output. However, this amount is minimized in this study to ensure high recovery rates.

3.2. Compression and purification unit 2

The CPU-2 is a modification of the CPU-1 used in the Allam cycle with similar design assumptions. In contrast to CPU-1 the CO_2 extracted from the power cycle and sent to the CPU-2 (stream 1) is liquid. Therefore, lower amount of cooling is needed to liquify the feed before entering the column. The corresponding process flow diagram is illustrated in Fig. 5. The values of the streams are provided in SI in Table S7. The modification consists of eliminating the second throttle valve after stream 6 at the recuperator (VLV-3, Fig. 4) Furthermore, the recuperator's cooling requirement is low, so the pure CO_2 liquid (stream 8) does not completely evaporate at the recuperator's outlet (see section 5.4). Consequently, a flash drum (FL-2) is added to separate the gaseous from the liquid. The liquid product is then pumped, and the gaseous product is compressed to 110 bar and cooled while heating the waste stream (stream 9). The product streams are mixed directly at high pressure. Similar to CPU-1, the hot waste stream then flows through a turbine to generate power and is subsequently vented to the atmosphere (stream 10).

Stream 8 consists of 74 % liquid, thereby adding flash drum (FL-2) to split the two-phase stream. The CO_2 purified aligns with ISO 27913 for dense phase pipeline transportation [27]. Stream Summary of the numerated streams is provided in Table S7 in SI.

4. Modeling and evaluation metrics

4.1. Thermodynamic models

The process simulations were performed using the equation-oriented AVEVA® Process Simulation (APS) software. The Peng Robinson equation of state was applied for the main power cycle, consistent with previous studies [17,24,28]. The PSRK equation of state was applied for modeling the CPU, the recycle liquefaction, and the water condensation in HX-WT-1. To ensure accuracy, the thermodynamic models were validated in-house against experimental data from literature. The validation covered binary mixtures of CO_2 with O_2, Ar, N_2, and H_2O, focusing on density and vapor–liquid equilibrium (VLE) evaluation.

The results confirmed that the Peng Robinson model provided reliable predictions of density across the investigated temperature and pressure ranges, with a maximum relative average deviation of approximately 5 % (see section 1.2.2 in SI, Table S14-S17). The PSRK model yielded the best agreement for VLE (see section 1.2.2 in SI, Fig. S1-S2).

Further validation of the modeled NG-fueled Allam process was conducted against the literature [28]. Based on the same NG-fuel mass flow, the energy consumption of the equipment and streams was benchmarked, and the deviation was calculated, with most values under 2 % (see section 1.2.1 in SI, Table S11-S13).

4.2. Power cycles

The composition of the fuel-grade DME used in this study is listed in Table S3 in SI and aligns with DIN TS 51698 [43] and trace impurities are considered within these specification limits. The total thermal input was fixed at 1,536 MW_{th}, in line with prior studies [19]. The oxygen feed is assumed to be supplied by an air separation unit at 99.5 mol % purity (Table S3 in SI), represented by a specific energy demand of 1,390 kJ/kg_{O2} aligned with [19,28]. A comparative review of oxygen production methods and associated energy requirements for different purities is also provided in the supplementary information (Table S9). In addition, key modeling assumptions are summarized in Table 2, while detailed assumptions, such as equipment pressure drop and machine efficiencies, are listed in supplementary (Table S1-S4). The assumptions used in this work align with reference literature [19,28] and they were applied to all modeled cycles to ensure a fair performance-focused benchmark.

The main recuperator (REC) was modeled as a multi-stream heat exchanger with 15 discretization elements to capture the nonlinear variation of thermophysical properties. The calculations were conducted to achieve a minimum pinch point temperature difference of 5 °C [28,44] while the turbine cooling flow exiting the recuperator was set to 183 °C. Since the software is equation oriented, both, cold- and hot-outlet were calculated. The additional heat supplied from the ASU is represented by a hot air stream at a temperature of 273 °C and pressure of 7.5 bar (see Table S3 in SI), that passes by the multi-stream recuperator as additional hot stream. The mass flow of the hot air stream is calculated based on oxygen to air mass ratio of 22.22 % [19].

The turbine cooling model followed Scaccabarozzi et al.'s approach [19,28] using 15 expansion steps to capture the continuous cooling of turbine blades. The combustor was modeled as a full-conversion reactor, assuming complete oxidation of all carbon-containing species in the fuel to CO_2 and H_2O (see Table S3 in SI).

To compare the technical and environmental performance of the cycles, this work uses three metrics. The first is net plant electrical efficiency, defined as the ratio of net power output P_{net} to the heat input $\dot{Q}_{in}$ on an lower heating value (LHV) basis (see Table S3 in SI), expressed in Eq. (1) and referred to as net efficiency in this work. The efficiency accounts for the power consumption of the CPU, ASU, and, in the case of the LiRAC, the VCU (cf. Eq. (2)).

$$\eta_{net,Allam} = \frac{P_{net}}{\dot{Q}_{in}} = \frac{\left(\left(P_T{*}\eta_m - \frac{\sum P_{C,RCL}}{\eta_m}\right){*}\eta_{gen}{*}\eta_{tr} - \frac{\sum P_P}{\eta_m} - \frac{P_{C,fuel}}{\eta_m} - P_{ASU} - P_{net,CPU}\right)}{\dot{m}_{fuel}{*}LHV_{fuel}} \quad (1)$$

Table 2
Key assumptions used in the cycle simulations.

Parameter	Value	Unit
Thermal energy of feedstock (LHV basis)	1,536	MW_{th}
Turbine inlet temperature	1,150	°C
Turbine inlet pressure	300	bar
Turbine outlet pressure	34	bar
Pinch point temperature difference	5	°C
Minimum achievable temperature by water cooling	26	°C
Maximum blade temperature	860	°C

$$\eta_{\mathrm{net,LiRAC}} = \frac{P_{\mathrm{net}}}{\dot{Q}_{\mathrm{in}}} = \frac{\left(P_{\mathrm{T}}*\eta_{\mathrm{m}}*\eta_{\mathrm{gen}}*\eta_{\mathrm{tr}} - \frac{\sum P_{\mathrm{P}}}{\eta_{\mathrm{m}}} - \frac{P_{\mathrm{C,fuel}}}{\eta_{\mathrm{m}}} - \frac{\sum P_{\mathrm{C,VCU}}}{\eta_{\mathrm{m}}} - P_{\mathrm{ASU}} - P_{\mathrm{net,CPU}}\right)}{\dot{m}_{\mathrm{fuel}}*LHV_{\mathrm{fuel}}} \quad (2)$$

The turbine mechanical power is defined as:

$$P_{\mathrm{T,m}} = P_{\mathrm{T}}*\eta_{\mathrm{m}} \quad (3)$$

The turbine electrical power output is calculated as:

$$P_{\mathrm{T,el_{out,LiRAC}}} = P_{\mathrm{T,m}}*\eta_{\mathrm{gen}}*\eta_{\mathrm{tr}}$$

$$P_{\mathrm{T,el_{out,Allam}}} = \left(P_{\mathrm{T}}*\eta_{\mathrm{m}} - \frac{\sum P_{\mathrm{C,RCL}}}{\eta_{\mathrm{m}}}\right)\eta_{\mathrm{gen}}*\eta_{\mathrm{tr}} \quad (4)$$

The compressors and pumps electrical power are defined as:

$$P_{\mathrm{P/C,el}} = \frac{P_{\mathrm{P/C}}}{\eta_{\mathrm{m}}} \quad (5)$$

In addition to net plant efficiency, an efficiency metric that excludes CPU power consumption is used to assess the energy penalty of CO_2 conditioning (cf. Eq. (6)).

$$\eta_{\mathrm{net_{excl.CPU}}} = \frac{\left(P_{\mathrm{net}} + P_{\mathrm{net,CPU}}\right)}{\dot{m}_{\mathrm{fuel}} \cdot LHV_{\mathrm{fuel}}} \quad (6)$$

To benchmark the cycles based on the carbon efficiency, the carbon capture rate (R_{CC}) is defined as the ratio of the captured and purified CO_2 to the total mass flow of CO_2 imported and generated $\dot{m}_{\mathrm{CO2,fuel,stoich}}$ (cf. Eq. (7) and (8)).

$$R_{\mathrm{CC}} = \frac{\dot{m}_{\mathrm{CO2,purified}}}{\dot{m}_{\mathrm{CO2,fuel,stoich}}} \quad (7)$$

$$\dot{m}_{\mathrm{CO2,fuel,stoich}} = \dot{m}_{\mathrm{CO2,generated}} + \dot{m}_{\mathrm{CO2,input,fuel}} \quad (8)$$

Furthermore, the CO_2 emission intensity is used to assess the environmental performance. Intensity relates all direct CO_2 emissions to net power output. This metric includes CO_2 emissions from the CPU ($\dot{m}_{\mathrm{CO2,Vent,CPU}}$) and CO_2 dissolved in water condensate from power cycles (cf. Eq. (9)). The dissolved CO_2 is not further recovered and is considered as emissions.

$$CO_2\ \text{emission intensity} = \frac{\dot{m}_{\mathrm{CO2,Vent,CPU}} + \dot{m}_{\mathrm{CO2,dissolved}}}{P_{\mathrm{net}}} \quad (9)$$

4.3. Compression and purification unit

Both CPU configurations were configured with similar design assumptions and optimized to achieve an oxygen concentration in the purified CO_2 below 10 ppm mol while maximizing the recovery rate up to 98 %. The minimum process temperature in the CPUs was limited to −55 °C to prevent dry-ice formation, specifically for the streams after each throttle valve and column top. The distillation column was modeled using 6 equilibrium stages with a pressure drop of 0.05 bar/stage, without hydrostatic pressure calculations. Additional design parameters and assumptions are summarized in Table S5 in SI. The purified CO_2 product fulfills the specifications for pipeline dense phase transport according to ISO 27913 [27].

To assess the performance of the CPUs, two essential metrics were used. First is the recovery rate (RR_{CPU}), which reflects the CPU's separation efficiency (cf. Eq. (10)).

$$RR_{\mathrm{CPU}} = \frac{\dot{m}_{\mathrm{CO2,purified}}}{\dot{m}_{\mathrm{CO2,feed,CPU}}} \quad (10)$$

Second, the specific work of the CPU (w_{CPU}) was used to benchmark the energetic performance. This metric quantifies the amount of net power consumed per unit of purified CO_2 (Eq. (11)), thus enabling a technical comparison independent of the system size.

$$w_{\mathrm{CPU}} = \frac{P_{\mathrm{net,CPU}}}{\dot{m}_{\mathrm{CO2,purified}}} = \frac{\left(-P_{\mathrm{T,CPU}}*\eta_{\mathrm{m}} + \frac{\sum P_{\mathrm{C,CPU}}}{\eta_{\mathrm{m}}}\right)}{\dot{m}_{\mathrm{CO2,purified}}} \quad (11)$$

4.4. Vapor compression unit

The VCU is modeled as an integrated subsystem coupled directly to the power cycle. The refrigerant mass flow and throttle-valve pressure drop were adjusted to fully liquefy the recycle stream (stream 7, Fig. 4) in the evaporator of the VCU while keeping a pinch point temperature difference of 2 °C. The refrigerant used consists of the same specifications of the fuel-grade DME listed in Table S3 in SI.

The coefficient of performance (COP) of the VCU was used to quantify the VCU's performance. This metric quantifies the amount of beneficial heat, i.e., evaporator duty per net power consumed by the compressors (cf. Eq. (12)).

$$COP = \frac{Duty_{\mathrm{VCU,evaporator}}}{\sum P_{\mathrm{C}}/\eta_{\mathrm{m}}} \quad (12)$$

5. Results and discussions

A comparative performance analysis for the DME-fueled Allam and the LiRAC is provided in section 5.1. In addition, the processes are benchmarked against literature results and own calculations for NG-fueled Allam cycle. Further analyses are conducted with focus on the overall energy and mass balance of both systems. Finally, a detailed analysis for the VCU and CPU is conducted to assess their performance.

To ensure a fair comparison between the Allam and LiRAC, a fixed heat input of 1,536 MW_{th} is set, and process parameters were kept similar. As a result, the simulation yield identical DME and oxygen feed mass flows of 53.24 kg/s and 111.80 kg/s, respectively, as well as an identical hot-air mass flow 502.29 kg/s.

5.1. Performance analysis of the simulated cycles

The performance analysis of the Allam cycle and the LiRAC is based on efficiency, carbon capture rates and CO_2 intensity. To ensure consistency and avoid discrepancies when comparing DME with NG from different literature sources and simulation tools, a NG-fueled Allam cycle was also simulated as part of this work. The resulting key performance indicators (KPIs) are listed in Table 3. In addition, a direct comparison with values reported in the studies by the IEAGHG [12] and Scaccabarozzi et al [28] is provided. An extended KPI table is included in the supplementary (Table S8).

The results show that the Allam cycle has a slightly higher net efficiency than the LiRAC (see Table 3). This difference could potentially be attributed to the higher hot side temperature achieved by recuperation in the Allam cycle, as discussed further in section 5.2.1.

Similar efficiencies were simulated between DME (50.4 %) and NG-fueled Allam cycle (50.3 %) in this work. The DME-fueled cycle exhibits an advantage in the ASU power demand. Since DME contains oxygen in its molecular structure, less external oxygen is required for the stoichiometric combustion per unit of heat input. In this work, the values are 0.072 $kg_{\mathrm{O2}}/MW_{\mathrm{th}}$ for DME-fueled and 0.08 $kg_{\mathrm{O2}}/MW_{\mathrm{th}}$ for NG-fueled Allam cycle. However, this advantage is offset by the higher CPU feed mass flow in the DME-fueled Allam cycle, which increases CPU power demand. Excluding the CPU power demand, the DME-fueled Allam cycle achieves a slightly higher efficiency of 53.5 %, compared to 52.9 % for the NG-fueled Allam cycle.

Compared to the results from literature, the IEAGHG study indicates

Table 3
Key simulation outcomes and comparative performance indicators of the investigated cycles compared with literature data.

Source		This work	This work	This work*	IEAGHG [19]	Scac. et. al* [28]
Fuel		DME	DME	NG	NG	NG
Process	Unit	LiRAC	Allam	Allam	Allam	Allam
Energy Performance						
Net efficiency	%	48.7	50.4	50.3	55.1	54.6
Net efficiency excl. CPU	%	49.4	53.5	52.9	56.0	–
Thermal energy LHV	MW_{th}	1,536.0	1,536.0	1,536.0	1,536.0	768.3
Net power output	MW_e	748.5	774.8	773.2	848.4	419.3
CPU power	MW_e	10.2	46.9	39.9	12.4	no CPU
ASU Power	MW_e	155.4	155.4	171.0	171.0	85.5
Carbon Performance						
Effective carbon capture	%	96.0	96.6	94.9	90.0	–
CPU recovery rate	%	98.9	98.9	97.7	90.0	–
CO_2 emission intensity	kg/MW_h	19.6	16.1	20.8	36.8	–
CO_2 emission intensity excl. CO_2 dissolved	kg/MW_h	5.2	5.1	9.1	36.8	no CPU
Mass Flows						
Fuel	kg/s	53.2	53.2	33.0	33.0	16.6
Oxygen	kg/s	111.8	111.8	123.0	123.0	61.5
CO_2 purified	kg/s	97.7	98.4	83.1	–	–
CO_2 gaseous emissions	kg/s	1.1	1.1	2.0	10.0	no CPU
Total CO_2 ($\dot{m}_{CO2,fuel,stoich}$)	kg/s	101.8	101.8	87.5	–	–
CO_2 dissolved	kg/s	3.0	2.4	2.5	–	–
Recycled stream	kg/s	2,537.0	2,570.2	2,582.3	2,663.2	1,353.9

This work*: Same design as DME-fueled Allam. Fuel composition of 89 vol% NG as in [19].
Scac. et. al*: Thermal energy considered as one train of 768.3 MW_{th} (half of the considered value in this work and in [19]).

higher efficiency for the NG-fueled Allam cycle. This can be explained by the lower CPU power demand in the report, which is based on 90 % recovery rate and an oxygen impurity of 0.01 mol % in purified CO_2. In addition, small discrepancies are to be expected due to differences in simulation software, thermodynamic models and the basis of design assumptions for turbomachinery. A direct comparison with the work of Scaccabarozzi et al. [28] based on the same NG-fuel mass flow is provided in the supplementary (Table S11-S13).

All cycles considered in this work achieved carbon capture rates of approximately 96 %. The DME-fueled Allam cycle demonstrates the lowest CO_2 emission intensity at 16.1 kg_{CO2}/MW_h, slightly below the LiRAC at 19.6 kg_{CO2}/MW_h and the NG-fueled Allam cycle at 20.8 kg_{CO2}/MW_h. The higher emission intensity in the NG-fueled cycle arises from the marginally higher CO_2 emitted, resulting from slightly lower CPU recovery rates. The lower recovery rate is due to the slightly lower CPU-feed CO_2 purity. Nevertheless, the effective capture rates could be further enhanced to higher values if the CO_2 dissolved in the condensed water is recovered, thus potentially reducing the CO_2 emission intensities depending on the energetic impact of such a recovery [45].

For reference, the minimum reported CO_2 intensities for NGCC with post-combustion capture are in the range of 30 kg_{CO2}/MW_h [15,16]. With the CO_2 product conditioned for enhanced oil recovery, literature reports a net efficiency of 53 %, a capture rate of 90 %, and a CO_2 intensity of 38 kg_{CO2}/MW_h [14]. Further purification of the CO_2 product to align with the pipeline specifications used in this work would also lead to a further decrease in the efficiency of the NGCC-PCC.

Overall, the findings position DME as a potential fuel for Allam-based power cycles without significant differences in efficiency compared to NG-fueled Allam. The LiRAC proves feasibility, exhibiting only 1.7 % lower efficiency than the Allam cycle, with potential for both further design optimization and benefits in dynamic operation.

5.2. Detailed comparison of the LiRAC and DME-fueled Allam cycle

To assess the differences in the efficiencies between the Allam and the LiRAC, a rigorous analysis of the heat recuperation, mass balance and energy balance has been conducted. The cycles are set to achieve same combustor temperature and same turbine outlet pressure leading to similar turbine outlet temperature of 742 °C entering the recuperator.

5.2.1. Heat recuperation

In the LiRAC, the recycled stream is liquefied at the lowest cycle pressure −11 °C and further pumped to the maximum pressure. As a result, the high pressure recycle stream 9 enters the recuperator at a temperature of 11 °C, compared to 50 °C in the Allam cycle. The difference is evident in the pressure enthalpy diagram in Fig. 2, where Allam cycle and LiRAC show distinct trajectories between points 7 and 9.

To evaluate the implications of the differences in temperatures on the heat transferred in the recuperator, temperature and duty (T-Q) diagrams of the recuperator for each cycle are visualized in Fig. 6.

As illustrated in Fig. 6, the T-Q curves of both recuperators show a nearly parallel and well-matched trend between the cold and hot curves, and the temperature approach remains narrow throughout, indicating effective heat transfer.

However, a steep change is observed in the T-Q curves of the Allam and LiRAC recuperators. This behavior is caused by the condensation of water in the hot stream (turbine exhaust). The difference in the position of the steep change between the two recuperators is potentially linked to the slight difference in water amount and, consequently, boiling temperature.

Additionally, the release of latent heat during water condensation increases the temperature driving force and allows further heat to be transferred. In the Allam recuperator, the 5 °C pinch point is reached at the beginning of condensation inside the recuperator, while for the LiRAC, the pinch point is shifted to the end of the recuperator's cold side.

Moreover, the LiRAC recuperates additional heat due to the lower inlet temperatures of the cold streams. Nevertheless, the cold outlet streams directed to the combustors in the LiRAC remains 7 °C colder than those in the Allam cycle. Due to the lower inlet temperature, the hot exhaust outlet cooled further, reaching 11.4 °C compared to 47.1 °C in the Allam cycle.

The findings indicate that the recuperators behave similarly in the two cycles. The only difference is the cold inlet in the LiRAC, which leads to a lower achievable recycle diluent temperature before entering the combustor and a colder exhaust exiting the recuperator.

5.2.2. Mass flows breakdown

The impact of the lower recycle temperature in the LiRAC is clearly

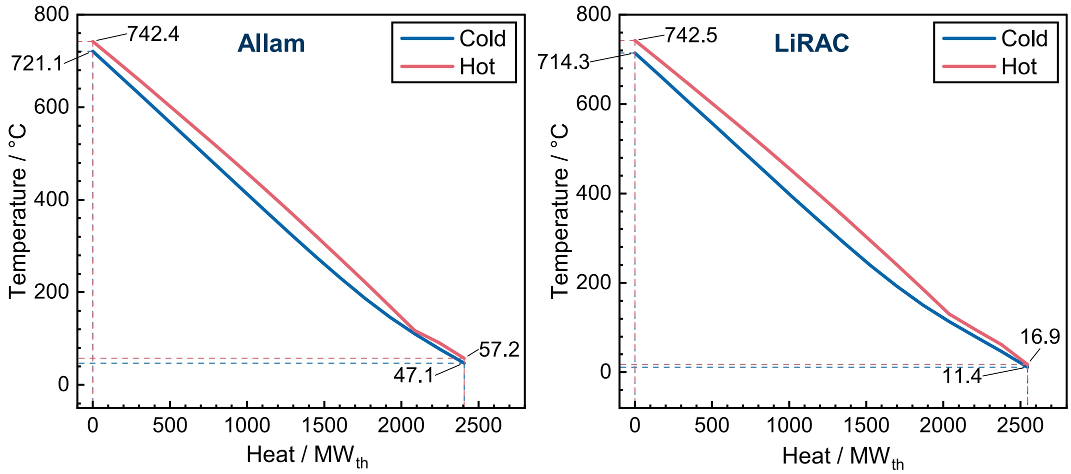

Fig. 6. Temperature-heat (T–Q) curves of the main power cycle recuperator (REC). Left: Allam cycle; right: LiRAC. Both cycles are simulated with same DME and O_2 assumptions for a fixed 1,536 MW_{th} heat input.

reflected in the reduced recycle mass flow, as illustrated in Fig. 7. The recycled flow amounts to 2,570.0 kg/s for the Allam cycle and 2,536.8 kg/s for the LiRAC. The lower temperature entering the combustor decreases the recycled diluent mass flow needed to maintain the target combustor temperature.

Further differences are observed in the captured CO_2 and condensed water streams. The total amount of water separated in the LiRAC is 65.5 kg/s, which is slightly higher than in the Allam cycle (64.8 kg/s).

In the Allam cycle a higher amount of CO_2 is captured, at 98.3 kg/s compared to 97.7 kg/s for the LiRAC. The difference of 0.62 kg/s is nearly equal to the difference in CO_2 dissolved in the separated water, which is 2.99 kg/s for the LiRAC and 2.37 kg/s for the Allam cycle. The difference in the amounts of condensed water and CO_2 dissolved is attributed to the additional drying step and the lower condensing temperature (stream 6, Fig. 1) in the LiRAC.

In conclusion, the temperature of the recycled diluent entering the combustor impacts the mass flow of the recycle and the overall mass flow in the system. Additionally, the lower recuperator cold inlet cooling the turbine exhaust to a lower temperature, as in the case of the LiRAC, results in more CO_2 dissolving in the water. Consequently, the CO_2 capture rate is lower since the dissolved CO_2 is not recovered.

5.2.3. Energy flows breakdown

The energetic implications of the lower recycled mass flows in the LiRAC are evident in the turbine power output, as shown in Fig. 8. The overall mass flow through the turbine decreases, resulting in lower turbine mechanical power output. Accordingly, the turbine delivers 1,206.8 MW in the LiRAC and 1,222.1 MW in the Allam cycle.

The LiRAC's main distinguishing features are the VCU and the liquid working medium. The compressors of the VCU in the LiRAC consume 175.7 MW_e, which exceeds the power consumption of the recycle compressors in the Allam cycle (130.8 MW_e). This difference is due to two factors. Firstly, the VCU compressors have a lower isentropic efficiency compared to the recycle compressors (Table S1). Secondly and predominantly, the refrigeration cycle has a higher pressure ratio of 4.4, compared to the recycle compressor's ratio of 3.05 (see section 5.3).

Conversely, the oxidant pump requires less power in the LiRAC (26.6 MW_e) than in the Allam cycle (34.1 MW_e). This reduction is due to the pump's higher inlet density (924.5 kg/m^3), which is caused by the lower temperature in the LiRAC case (−5.5 °C).

Clearly, CPU-1 (Allam) requires substantially more energy (36.7 MW_e) than CPU-2 (LiRAC), mainly due to the liquid feed in CPU-2 (see section 5.4).

Taking all these differences into account, the total net power output difference between the LiRAC and Allam cycles is 26 MW_e, mainly due to the lower power generated through the turbine.

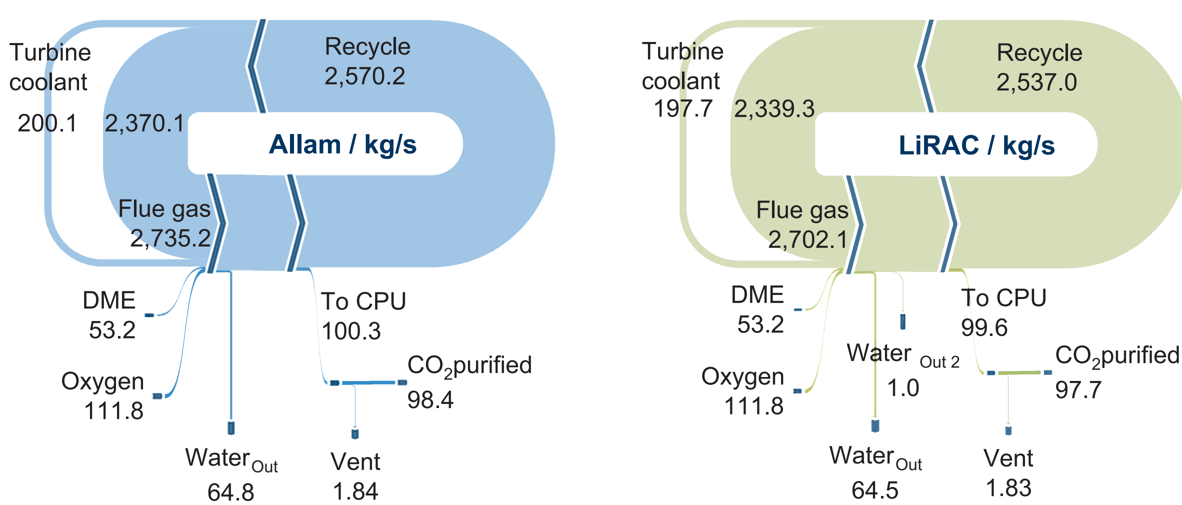

Fig. 7. Mass flow Sankey diagrams for the Allam cycle (left) and the LiRAC (right). Both cycles are simulated with same DME and O_2 feed assumptions for a fixed 1,536 MW_{th} heat input.

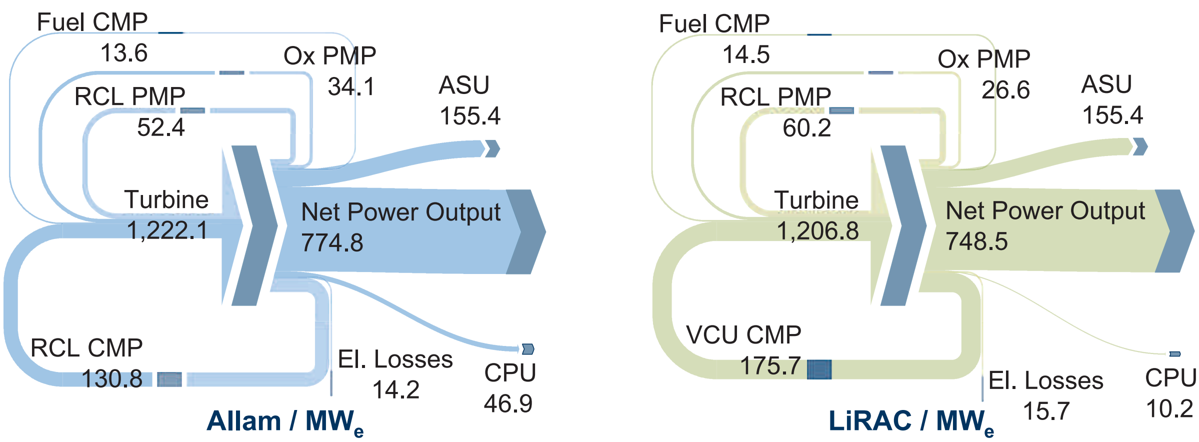

Fig. 8. Energy Sankey diagrams for the Allam cycle (left) and the LiRAC (right). "El. Losses" represent the turbine losses exhibited by the generator and transformer on the turbine mechanical power output. Both cycles are simulated with same DME and O_2 feed assumptions for a fixed 1,536 MW_{th} heat input.

5.3. Thermodynamic analysis of the VCU

The VCU in the LiRAC requires 175.7 MW_e of power, which is significant and higher than the Allam cycle's recycle compressor's power demand. Fig. 9 illustrates the VCU's process flow and corresponding pressure-enthalpy diagrams and the T-Q Curves of the evaporator. The values of the numbered streams in the figures are listed in Table 4.

A defining feature of the LiRAC configuration is the use of the fuel-grade DME itself as the refrigerant within the VCU. The simulation results indicate high refrigerant effectiveness. Specifically, the refrigerant mass flow ratio (stream 4) to the recycled CO_2 mixture (stream 7) is 0.68, which is 32 % lower than the recycled stream. This reduction is due to DME's higher enthalpy of vaporization relative to that of the recycled CO_2 mixture.

The VCU achieves a COP of 4.2, with a cycle pressure ratio of 4.4. This pressure ratio results from the required condensation temperature of 26 °C and the evaporation temperature of - 12 °C (1.79 bar). These operating conditions and limitations depend on the thermophysical properties of the refrigerant, specifically the composition of the fuel-grade DME. The condensation temperature is defined by the cooling water, and the evaporation temperature depends on the recycled CO_2 mixture and the required temperature difference in the evaporator to ensure heat transfer.

The recycled CO_2 mixture (stream 7) enters at 16 °C and begins to liquefy at around − 4 °C (cf. Fig. 9). The phase change occurs quasi-isothermally up to 600 MW_{th} of transferred heat. Then, the temperature decreases sharply to −10 °C, at which stream 7 is fully liquefied. The sharp temperature drop is likely caused by inert components in the CO_2 mixture that shift the boiling temperature to lower temperatures at higher liquid fractions. Altogether, 739 MW_{th} of cooling duty is required to fully liquefy the recycled CO_2 mixture (stream 7 to stream 7*).

In summary, improving the efficiency of the LiRAC relies heavily on reducing the energy consumption of the VCU compressors. This can be achieved by minimizing the pressure ratio of the VCU and thus lowering the compression work.

5.4. Energy breakdown of the CPUs

The compression and purification units account for a significant portion of the energy consumption. The energy analysis shows that the CPU-1 (Allam) required more energy than CPU-2 (LiRAC).

In CPU-1, the incoming feed is fully gaseous and requires 51.6 MW_{th} (Fig. 10) of cooling to achieve liquid fraction of 0.23 before entering the reboiler (stream 3, Fig. 4). In contrast, CPU-2's incoming stream is partly liquid (stream 2, Fig. 5), achieving a higher liquid fraction of 0.59 with lower cooling demand (9.7 MW_{th} Fig. 10). Consequently, the throttled column feed (stream 4) exhibits a higher vapor fraction in CPU-1 of 0.78 compared to 0.45 in CPU-2.

The higher vapor fraction increases the gaseous flow at the top of the column. This results in larger CO_2 losses, higher recycled mass flows, and ultimately, higher energy consumption in CPU-1. Specifically, CPU-1's recycled mass flow of 319.88 kg/s results in an energy demand of 25.67 MW_e, whereas CPU-2's recycled mass flow of 73.09 kg/s results in a lower demand of only 5.68 MW_e. In both CPUs, more than 50 % of the total energy is consumed in the recycling compression step.

According to Eq. (8), the specific energy consumption is 476.73 kJ/

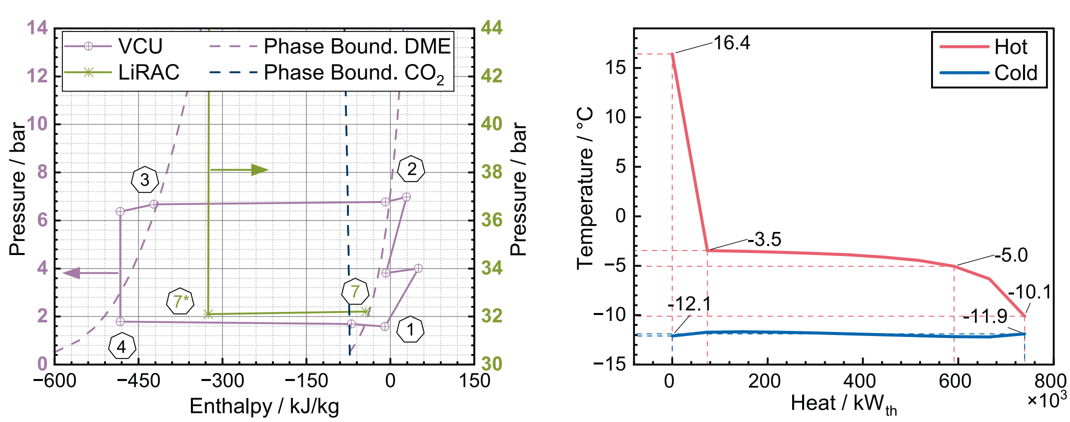

Fig. 9. Left: Pressure-enthalpy diagram of the VCU with the liquefaction of the recycle CO_2 mixture (green). Right: Temperature-heat (T-Q) curve of the VCU evaporator in the LiRAC.

Table 4
Stream values of the vapor compression unit.

Stream Nr.	Unit	1	2	3	4	7	7*
$\dot{m}$	kg/s	1,790.1	1,790.1	1,790.1	1,790.1	2,636.6	2,636.6
$\dot{V}$	m^3/s	584.3	138.4	2.6	30.9	35.9	2.7
T	°C	21.0	55.3	26.0	−12.1	16.4	−10.1
p	bar	1.6	7.0	6.7	1.8	32.2	32.1
ρ	kg/m^3	3.1	12.9	681.8	57.9	73.5	991.8
VF	–	1.0	1.0	0.0	0.1	1.0	0.0
DH	kJ/kg	−9.6	29.1	−422.5	−482.5	−43.9	−324.2
				Composition in mol %			
CO_2		0.10	0.10	0.10	0.10	99.04	99.04
O_2		0.00	0.00	0.00	0.00	0.19	0.19
Ar		0.00	0.00	0.00	0.00	0.46	0.46
N_2		0.00	0.00	0.00	0.00	0.31	0.31
CO		0.02	0.02	0.02	0.02	0.00	0.00
H_2O		0.08	0.08	0.08	0.08	0.00	0.00
CH_3OH		0.07	0.07	0.07	0.07	0.00	0.00
DME		99.12	99.12	99.12	99.12	0.00	0.00
CH_4		0.14	0.14	0.14	0.14	0.00	0.00
Ethane		0.23	0.23	0.23	0.23	0.00	0.00
Propane		0.10	0.10	0.10	0.10	0.00	0.00
Butane		0.08	0.08	0.08	0.08	0.00	0.00
Formic acid		0.05	0.05	0.05	0.05	0.00	0.00

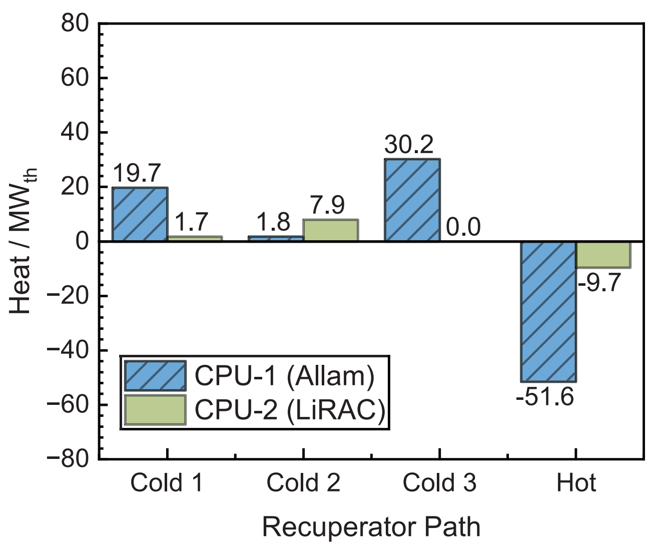

Fig. 10. Heat transferred in the recuperator of the CPUs.

kg_{CO2} for CPU-1, which is higher than for CPU-2 (104.35 kJ/kg_{CO2}). Moreover, CPU-2 requires 4.76 MW_e to pressurize the purified CO_2 to pipeline pressure, which is lower than CPU-1′s demand of 21.5 MW_e. This lower energy demand is due to the liquid fraction (0.74) of the purified stream (stream 8), which enables some of the CO_2 to be pumped as a liquid, while only the remaining vapor is compressed. Notably, the liquid purified CO_2 (stream 8) could potentially be provided for shipping instead of being pressurized for the pipeline [12].

Overall, CPU-2′s feed is in a more favorable thermodynamic state, which explains its significantly lower energy demand compared to CPU-1.

6. Conclusion and outlook

In this study, we performed a detailed thermodynamic analysis of DME as a fuel in two oxy-combustion sCO_2 power cycles. Specifically, we conducted a detailed comparison of the DME-fueled Allam cycle with the novel cycle introduced in this work: the Liquefied Recycle Allam Cycle (LiRAC). The LiRAC is a modified Allam cycle that integrates a vapor compression unit with fuel-grade DME as the refrigerant, enabling the complete liquefaction of the working medium. Furthermore, we benchmarked the DME-fueled cycles and NG-fueled Allam cycle under aligned assumptions. Additionally, we provided an extensive analysis of the energy requirements for the compression and purification units used to achieve high capture rate and to ensure that captured CO_2 meets transport specifications.

Both cycles demonstrated high performance, achieving net efficiencies of 50.4 % (Allam cycle) and 48.7 % (LiRAC) and effective CO_2 capture rates above 96 %, approaching carbon neutrality. For reference, we simulated an NG-fueled Allam cycle under equivalent boundary conditions. The results showed nearly identical efficiency compared to the DME-fueled cycle. Regarding environmental performance, the direct CO_2 emission intensities are close for both DME-fueled cycles under 19.6 kg_{CO2}/MW_h, thus lower than the minimum of 30 kg_{CO2}/MW_h reported for NGCC with post-combustion carbon capture [14–16]. Moreover, the captured CO_2 in all cycles is pipeline-ready and meets the oxygen impurity limit of less than 10 ppm mol. Consequently, direct deployment and a nearly closed carbon loop are feasible when the captured CO_2 is reused for DME-synthesis.

These findings position DME-fueled Allam-based cycles as a potential path for efficient and sustainable power generation. However, challenges remain regarding materials that can withstand degradation under high-pressure, high-temperature conditions and in reactive working fluid mixtures. Therefore, it is crucial to develop cost-competitive equipment that can operate under such conditions and ensure a cost-competitive renewable fuel feedstock (i.e., DME) to enable competitive electricity costs.

Future work should assess DME performance in the combined cycle gas turbine with post-combustion carbon capture under aligned boundary conditions (i.e., high capture rates and high CO_2 purity) to enable fair benchmarking against oxy-combustion sCO_2 cycles. The minor efficiency gap between the Allam and LiRAC cycles highlights the feasibility of the LiRAC. Therefore, further investigation should focus on optimizing the cycle and investigating part-load operation, as well as exploring further potential benefits and applications of the LiRAC.

7. Declaration of generative AI and AI-assisted technologies in the manuscript preparation process

During the preparation of this work the authors used DeepL and ChatGPT in order to improve language. After using these services, the authors reviewed and edited the content as needed and take full responsibility for the content in this paper.

CRediT authorship contribution statement

Ghadi Abi Haidar: Writing – original draft, Visualization, Validation, Methodology, Investigation, Data curation, Conceptualization. **Philipp Morsch:** Writing – review & editing, Supervision, Methodology, Conceptualization. **Andreas Peschel:** Writing – review & editing, Supervision, Methodology.

Declaration of competing interest

The authors declare the following financial interests/personal relationships which may be considered as potential competing interests: Andreas Peschel has patent #EP4548015A1 pending to Forschungszentrum Juelich GmbH. Ghadi Abi Haidar and Philipp Morsch are employees of the patent assignee Forschungszentrum Juelich GmbH. If there are other authors, they declare that they have no known competing financial interests or personal relationships that could have appeared to influence the work reported in this paper.

Acknowledgements

The authors would like to acknowledge the funding by the German Federal Ministry of Research, Technology and Space (BMFTR) and the Ministry of Economic Affairs, Industry, Climate Action and Energy of the State of North Rhine-Westphalia through the project HC-H2.

Appendix A

Table A5
Stream summary of the simulated DME-fueled power cycles aligned with the numeration in the process flow diagram in Fig. 1.

		1*		2		3		4		5		6	
	Unit	Allam	LiRAC	Allam	LiRAC	Allam	LiRAC	Allam	LiRAC	Allam	LiRAC	Allam	LiRAC
$\dot{m}$	kg/s	53.2	53.2	1115.5	1116.6	1366.4	1334.6	2535.1	2504.4	2735.2	2702.1	2735.2	2702.1
T	°C	26.0	55.3	721.1	714.3	721.1	714.3	1150.1	1150.1	742.4	742.5	57.2	16.9
P	bar	5.8	7.0	303.4	303.4	303.4	303.4	300.0	300.0	34.0	34.0	33.2	33.2
						Composition in mol %							
CO_2		–	–	85.8	85.9	98.9	99.0	93.2	93.2	93.6	93.6	93.6	93.6
O_2		–	–	13.3	13.3	0.2	0.2	0.2	0.2	0.2	0.2	0.2	0.2
Ar		–	–	0.4	0.4	0.5	0.5	0.4	0.4	0.4	0.4	0.4	0.4
N_2		–	–	0.3	0.3	0.3	0.3	0.3	0.3	0.3	0.3	0.3	0.3
CO		–	–	0.0	0.0	0.0	0.0	0.0	0.0	0.0	0.0	0.0	0.0
H_2O		–	–	0.1	0.0	0.2	0.0	5.9	5.9	5.5	5.5	5.5	5.5
						Continued							
		7		8		9		10		11		12	
	Unit	Allam	LiRAC	Allam	LiRAC	Allam	LiRAC	Allam	LiRAC	Allam	LiRAC	Allam	LiRAC
$\dot{m}$	kg/s	2670.5	2636.6	2570.2	2537.0	1366.4	1334.6	1115.5	1116.6	200.1	197.7	1115.5	1116.6
T	°C	26.0	16.4	26.0	−2.4	50.1	11.4	47.1	11.9	183.0	183.0	17.5	−5.5
P	bar	32.8	32.2	120.0	120.0	305.0	305.0	305.0	305.0	303.4	303.4	120.0	120.0
						Composition in mol %							
CO_2		98.9	99.0	98.9	99.0	98.9	99.0	85.8	85.9	98.9	99.0	85.8	85.9
O_2		0.2	0.2	0.2	0.2	0.2	0.2	13.3	13.3	0.2	0.2	13.3	13.3
Ar		0.5	0.5	0.5	0.5	0.5	0.5	0.4	0.4	0.5	0.5	0.4	0.4
N_2		0.3	0.3	0.3	0.3	0.3	0.3	0.3	0.3	0.3	0.3	0.3	0.3
CO		0.0	0.0	0.0	0.0	0.0	0.0	0.0	0.0	0.0	0.0	0.0	0.0
H_2O		0.2	0.0	0.2	0.0	0.2	0.0	0.1	0.0	0.2	0.0	0.1	0.0

*: The composition of stream 1 is equivalent to that of the fuel DME listed in Table 3 in Supplementary information.

Appendix B. Supplementary data

Supplementary data to this article can be found online at https://doi.org/10.1016/j.enconman.2026.121439.

Data availability

The authors declare that the data supporting the findings of this study are available within the paper and its Supplementary Information.

References

[1] International Energy Agency. World Energy Outlook 2024; 2024.
[2] International Energy Agency. Electricity 2024 - Analysis and forecast to 2026; 2024.
[3] Federal Ministry for Economic Affairs and Climate Action. Import Strategy for hydrogen and hydrogen derivatives; 2024.
[4] Peschel A, Wasserscheid P. Perspective on the technology status of chemical hydrogen carriers for ship-based energy import. Electrochem Sci Adv 2026;6(1). https://doi.org/10.1002/elsa.70015.
[5] Ulrich O, Morsch P, Peschel A. Decentralized use case integration of chemical hydrogen carriers: the cost saving potential in domestic supply chains. Int J Hydrogen Energy 2025;186:151928. https://doi.org/10.1016/j.ijhydene.2025.151928.
[6] Schühle P, Stöber R, Gierse M, Schaadt A, Szolak R, Thill S, et al. Dimethyl ether/ CO_2 – a hitherto underestimated H 2 storage cycle. Energy Environ Sci 2023;16(7): 3002–13. https://doi.org/10.1039/D3EE00228D.
[7] Ruther T, Stadler H, Peschel A. Potential of high-temperature steam reforming for enabling DME as a hydrogen carrier. Chem Eng J 2025;524:168929. https://doi.org/10.1016/j.cej.2025.168929.
[8] Kim MY, Yoon SH, Ryu BW, Lee CS. Combustion and emission characteristics of DME as an alternative fuel for compression ignition engines with a high pressure injection system. Fuel 2008;87(12):2779–86. https://doi.org/10.1016/j.fuel.2008.01.032.
[9] Lee MC, Seo SB, Chung JH, Joo YJ, Ahn DH. Industrial gas turbine combustion performance test of DME to use as an alternative fuel for power generation. Fuel 2009;88(4):657–62. https://doi.org/10.1016/j.fuel.2008.10.027.
[10] Wood Group. Industry Guidelines for Setting the CO_2 Specification in CCUS Chains: Work Package 9 - Ship Transport; 2024.
[11] Mitsubishi Heavy Industries, Ltd. Liquefied CO_2 Carrier "EXCOOL": Mitsubishi Heavy Industries Technical Review Vol. 61 No. 2. Mitsubishi Heavy Industries Technical Review 2024;61(2).
[12] ISO/TR 27929. Transportation of CO_2 by ship; 2024.
[13] IEAGHG. CO_2 Capture at Gas Fired Power Plants, 2012/8, July, 2012.

[14] Turner M, Schmitt T, Oakes M, Konrade J, Bleckinger M, Sturdivan M. Cost and performance baseline for fossil energy plants. volume 3: low rank coal and natural gas to electricity. Pittsburgh 2023.
[15] IEAGHG. Towards Zero Emissions CCS in Power Plants Using Higher Capture Rates or Biomass 2019/02, March,2019.
[16] Edenhofer O, Pichs-Madruga R, Sokona Y, Minx JC, Farahani E, Kadner S et al. (eds.). Climate Change 2014: Mitigation of Climate Change ; Summary for Policymakers Technical Summary ; Part of the Working Group III Contribution to the Fifth Asessment Report of the Intergovernmental Panel on Climate Change. Geneva, Switzerland: Intergovernmental Panel on Climate Change; 2015.
[17] Allam R, Martin S, Forrest B, Fetvedt J, Lu X, Freed D, et al. Demonstration of the Allam cycle: an update on the development status of a high efficiency supercritical carbon dioxide power process employing full carbon capture. Energy Procedia 2017;114:5948–66. https://doi.org/10.1016/j.egypro.2017.03.1731.
[18] Brun K, Friedman P, Dennis R, editors. Fundamentals and Applications of Supercritical Carbon Dioxide (sCO_2) Based Power Cycles. Woodhead Publishing; 2017.
[19] IEAGHG. Oxy-Combustion Turbine Power Plants, 2015/05, August, 2015.
[20] Jokola G, Myhre r, Weizel P, Marasigan J, Maxson A. Oxy-combustion roadmap to commercialization. In: 15th International Conference on Greenhouse Gas Control Technologies, GHGT-15.
[21] Net Power Inc. La Porte Demonstration Facility: https://netpower.com/la-porte-demo-facility/. [January 12, 2026]; Available from: https://netpower.com/technology/#laporte.
[22] Rogalev N, Rogalev A, Kindra V, Zlyvko O, Bryzgunov P. Review of closed SCO_2 and semi-closed oxy–fuel combustion power cycles for multi-scale power generation in terms of energy, ecology and economic efficiency. Energies 2022;15 (23):9226. https://doi.org/10.3390/en15239226.
[23] Northern Lights. Liquid CO_2 (LCO_2) Quality Specifications. [January 12, 2026]; Available from: https://norlights.com/wp-content/uploads/2025/06/Liquid-specification-2306251.pdf.
[24] Martinelli M, Chiesa P, Martelli E. Techno-economic assessment of the Allam cycle for different plant sizes, oxygen purities and heat integration with external sources. Fuel 2025;381:133383. https://doi.org/10.1016/j.fuel.2024.133383.
[25] Giovanni M, Ahtasham R, Antonio F. Methanol-fired Allam cycle: combining oxy-fuel power cycles with synthetic e-fuels. In: Proceedings of ASME Turbo Expo 2024 Turbomachinery Technical Conference and Exposition.
[26] Dong X, Fang Z, Tang X, Qiao X, Li X, Zhou D, et al. Thermodynamic and exergoeconomic analysis of a dual expansion and triple recuperation supercritical CO_2 power cycle driven by DME-oxygen combustor. Energ Conver Manage 2024; 303:118173. https://doi.org/10.1016/j.enconman.2024.118173.
[27] ISO 27913. Carbon dioxide capture, transportation and geological storage - Pipeline transportation systems; 2024.
[28] Scaccabarozzi R, Gatti M, Martelli E. Thermodynamic analysis and numerical optimization of the NET Power oxy-combustion cycle. Appl Energy 2016;178: 505–26. https://doi.org/10.1016/j.apenergy.2016.06.060.
[29] Dago GGB, Frate GF, Baccioli A, Ferrari L, Alfarano E, Colnago A. Exergy analysis of the Allam cycle: assessing the impact of regenerator performance on the cycle efficiency. Energ Conver Manage 2025;345:120358. https://doi.org/10.1016/j.enconman.2025.120358.
[30] Moore JJ, Pryor O, Cormier I, Fetvedt J. Oxygen storage incorporated into net power and the Allam–fetvedt oxy-fuel sCO2 power cycle—techno-economic analysis. J Eng Gas Turbines Power 2024;146(9). https://doi.org/10.1115/1.4065048.
[31] Xu H, Xu C, Chen S, Dai T, Xin T, Yang Y. Development of an improved part-load operation strategy for the recompression semi-closed CO2 cycle. Energy 2025;334: 137746. https://doi.org/10.1016/j.energy.2025.137746.
[32] Fernandes D, Wang S, Xu Q, Chen D. Dynamic simulations of the Allam cycle power plant integrated with an air separation unit. Int J Chem Eng 2019;2019:1–10. https://doi.org/10.1155/2019/6035856.
[33] Viv A. Bone, Michael P. Kearney, Ingo H.J. Jahn. Towards model predictive control for supercritical CO2 cycles.
[34] Kumar A, Daoutidis P. Nonlinear dynamics and control of process systems with recycle. J Process Control 2002;12(4):475–84. https://doi.org/10.1016/S0959-1524(01)00014-2.
[35] Sinkevich M, Kosoy A, Popel O. Comparative analysis of the Allam cycle and the cycle of compressorless combined cycle gas turbine unit. E3S Web Conf 2020;209: 3023. https://doi.org/10.1051/e3sconf/202020903023.
[36] Yu H, Gundersen T, Gençer E. Optimal liquified natural gas (LNG) cold energy utilization in an Allam cycle power plant with carbon capture and storage. Energ Conver Manage 2021;228:113725. https://doi.org/10.1016/j.enconman.2020.113725.
[37] Posch S, Haider M. Optimization of CO_2 compression and purification units (CO_2CPU) for CCS power plants. Fuel 2012;101:254–63. https://doi.org/10.1016/j.fuel.2011.07.039.
[38] Sala L, Zaryab SA, Chiesa P, Martelli E. Comparison and optimization of CO_2 purification units for CCS applications. Int J Greenhouse Gas Control 2024;136: 104193. https://doi.org/10.1016/j.ijggc.2024.104193.
[39] White V, Allam RJ. Purification of carbon dioxide. European patent EP 1953486 B1; 2010.
[40] ISO 27913. Carbon dioxide capture, transportation and geological storage - Pipeline transportation systems; 2016.
[41] Chinello G, Arellano Y, Span R, van Putten D, Abdulrahman A, Joonaki E, et al. Toward standardized measurement of CO_2 transfer in the CCS chain. Nexus 2024. https://doi.org/10.1016/j.ynexs.2024.100013.
[42] ARAMIS. Specification for the CO_2 supplied: CCS-ARAMIS Project. ARM-CPT-BB8-PRO-MEM-0033 rev 6.2. [January 21, 2026]; Available from: https://www.aramis-ccs.com/files/13032025-ARM-CPT-BB8-PRO-MEM-0033-rev-6.2-public-version-NEW.pdf.
[43] DIN/TS 51698. Kraft- und Brennstoffe Anforderungen- Dimethylether (DME) 2022.
[44] Wimmer K, Sanz W. Optimization and comparison of the two promising oxy-combustion cycles NET Power cycle and Graz Cycle. Int J Greenhouse Gas Control 2020;99:103055. https://doi.org/10.1016/j.ijggc.2020.103055.
[45] Bocandé D, Rohardt J, Schatz M. The Hydrogen-Fueled Allam Cycle: Thermodynamic Evaluation and Optimization After a Fuel Switch to Hydrogen. In: ASME Turbo Expo 2025: Turbomachinery Technical Conference and Exposition.